Research article

S. Azar Oliaei Motlagh* and Vadym Apalkov

Anomalous ultrafast all-optical Hall effect in gapped graphene

https://doi.org/10.1515/nanoph-2021-0227
Received May 10, 2021; accepted July 30, 2021;
published online August 18, 2021

Abstract: We propose an ultrafast all-optical anomalous Hall effect in two-dimensional (2D) semiconductors of hexagonal symmetry such as gapped graphene (GG), transition metal dichalcogenides (TMDCs), and hexagonal boron nitride (h-BN). To induce such an effect, the material is subjected to a sequence of two strong-field single-optical-cycle pulses: A chiral pump pulse followed within a few femtoseconds by a probe pulse linearly polarized in the armchair direction of the 2D lattice. Due to the effect of topological resonance, the first (pump) pulse induces a large chirality (valley polarization) in the system, while the second pulse generates a femtosecond pulse of the anomalous Hall current. The proposed effect is fundamentally the fastest all-optical anomalous Hall effect possible in nature. It can be applied to ultrafast all-optical storage and processing of information, both classical and quantum.

Keywords: anomalous Hall effect; femtosecond pulse; graphene; laser pulse; pulse matter interaction; ultrafast process.

1 Introduction

Two-dimensional (2D) materials with honeycomb crystal structure [1], such as graphene, silicene, transition metal dichalcogenides (TMDCs), and hexagonal boron nitride (h-BN), possess nontrivial topological properties in the reciprocal space [2]. Such properties are determined by the Berry curvature, which is concentrated at the K and K' points of the Brillouin zone. While for graphene, which is a semimetal, the Berry curvature is singular at the K and K' points and zero elsewhere, in the gapped graphene [3] (GG) and semiconductor TMDCs the Berry curvature is regular in the entire Brillouin zone with extrema at the K and K' points. Consequently, the ultrafast electron dynamics produced by the strong optical pulses is fundamentally different in these materials [4, 5].

In graphene, for a single-oscillation chiral ("circularly polarized") pulse, the residual (left after the pulse) population of the conduction band (CB) is almost the same for the K and K' valleys (i.e., the induced valley polarization is very weak). For a longer pulse (with two or more optical oscillations), the valley polarization is larger; there are also pronounced fringes in the CB electron population, which form an electron interferogram caused by the accumulation of the Berry phase along the Bloch trajectories of electrons in the reciprocal space [4]. These interferograms possess characteristic forks manifesting the presence of a quantized Berry flux of $\pm\pi$. The electron CB population distribution in the reciprocal space for both linearly [6] and circularly-polarized pulses [4] are asymmetric, which causes electric currents that have been recently observed experimentally [7].

In stark contrast, the two-dimensional semiconductors (GG and TMDCs) placed in the field of chiral pulse, behave quite differently from graphene. Namely, there is a strong valley polarization induced by a circularly-polarized CW radiation of relatively low intensity [8–13]. A strong valley polarization can be introduced even by a single-oscillation ultrashort intense optical pulse [5]. The reason for a strong residual valley polarization in the two-dimensional semiconductors is that they have broken inversion symmetry and, consequently, a finite bandgap. As a result, for a chiral pulse that breaks the time-reversal ($\mathcal{T}$) symmetry, the valleys in the residual state of the system are populated differently. For a relatively weak CW fields, this asymmetry is due to the chiral selection rules of the transitional dipole at the K and K' points. For an intense single-oscillation pulse, the strong valley polarization is caused by the effect of topological resonance [5], which is

*Corresponding author: S. Azar Oliaei Motlagh, Department of Physics and Astronomy, Georgia State University, Atlanta, Georgia, 30303, USA, E-mail: soliaeimotlagh1@gsu.edu. https://orcid.org/0000-0002-6732-8946
Vadym Apalkov, Center for Nano-Optics (CeNO) and Department of Physics and Astronomy, Georgia State University, Atlanta, Georgia, 30303, USA

Open Access. ©2021 Azar Oliaei Motlagh and Vadym Apalkov, published by De Gruyter. This work is licensed under the Creative Commons Attribution 4.0 International License.

due to the interference of the topological phase (the sum of the Berry phase and the phase of the transitional dipole matrix element) and the dynamic phase.

Ultrafast generation of a large valley polarization in the GG and TMDCs by a single-oscillation chiral pulse opens up a possibility to observe an ultrafast anomalous all-optical Hall effect. The Hall current [14] can be realized only in systems with broken time reversal symmetry. For the conventional Hall effect, the time reversal symmetry is broken by an external magnetic field. In the systems, which show the anomalous Hall effect [15], the time reversal symmetry is broken even without an external magnetic field. Such anomalous Hall effect can be realized, for example, in TMDC monolayers with unbalanced population of photoexcited valleys [16, 17] or in semiconductor systems with photoinduced spin polarization and strong spin–orbit interaction [18]. In these systems, even without magnetic field, the time reversal symmetry is broken and under an applied DC electric field, the Hall current is generated. Such current is called an anomalous Hall current and it is usually probed by DC electric field. Here we propose to probe the broken time reversal symmetry of the system by an ultrashort optical pulse. Consider a second single-cycle optical pulse that is linearly polarized in the armchair direction incident normally on the already valley-polarized solid, where the valley polarization is generated by a single-oscillation chiral pulse. It is predicted to produce both a normal current in the direction of the electric field and the Hall current in the perpendicular (zigzag) direction. The latter is due to the net effect of the Berry curvature in the valley-polarized system. It changes sign for the chiral pulse of the opposite handedness. This normal current is the manifestation of the anomalous (without a magnetic field) all-optical Hall effect. The proposed all-optical anomalous Hall effect is the fundamentally fastest such an effect in nature: It takes just a single optical cycle to induce the large valley polarization and another single cycle pulse to read it out.

In this article, we consider GG, which is experimentally obtained by growing the graphene on a different substrate, i.e., on SiC [19, 20]. The GG can also serve as a generic model of TMDCs. We predict the generation of an anomalous Hall current by a combination of a strong chiral pulse, which breaks the time-reversal symmetry thus playing the role of an effective magnetic field, followed by a linearly polarized probe pulse. Using the model of GG allows one to model materials with different bandgaps and to study how the anomalous Hall effect depends on the magnitude of the bandgap.

2 Model and main equations

2.1 Time-dependent Schrödinger equation and its solution

A gap in graphene can be opened by breaking the inversion symmetry ($\mathcal{P}$), i.e., the symmetry between two sublattices [3], A and B. To describe the GG, we consider two-band tight-binding Hamiltonian, which includes an extra diagonal term with the on-site energies $\Delta_g/2$ and $-\Delta_g/2$ at two sublattices A and B, respectively – see Figure 1(a). This difference in the on-site energies breaks down the $\mathcal{P}$-symmetry causing the bandgaps of Δ_g to open up at the K- and K'-points – see the schematics of the Brillouin zone in Figure 1(b). Note that the electron spectra in the K and K' valleys are identical as protected by the time-reversal symmetry – see Figure 1(c), while the Berry curvatures are opposite.

Below we consider the interaction of the GG with ultrashort optical pulses for a few femtosecond duration. The electron scattering times in graphene and other 2D materials are on the order of or significantly longer than 10 fs – see Refs. [21–26]. For ultrashort optical pulses with the duration less than 10 fs we disregard the electron scattering processes and consider the electron dynamics in the field of the pulse as coherent and collisionless. Consequently, it can be described by a time-dependent Schrödinger equation (TDSE),

$$i\hbar\frac{\mathrm{d}\Psi}{\mathrm{d}t} = H_{\mathbf{k}}(t)\Psi, \quad H_{\mathbf{k}}(t) = H_{\mathbf{k}0} - e\mathbf{F}(t)\mathbf{r}, \tag{1}$$

where $H_{\mathbf{k}}(t)$ is the Hamiltonian of an electron system, which consists of the field-free Hamiltonian, $H_{\mathbf{k}0}$, and the interaction Hamiltonian with the field of the pulse, $-e\mathbf{F}(t)\mathbf{r}$. Here, $\mathbf{F}(t)$ is the pulse's electric field, e is electron charge,

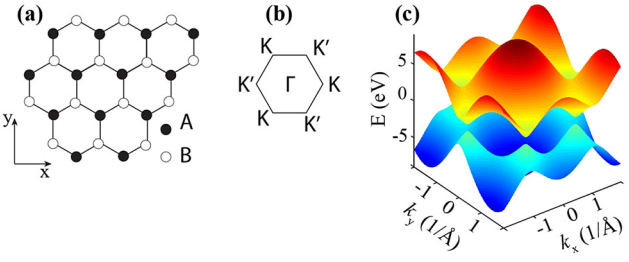

Figure 1: (a) Honeycomb crystal structure of graphene with sublattices A and B. (b) The first Brillouin zone of graphene with two valleys K and K'. (c) Energy dispersion a function of crystal wave vector for GG with the band gap of 1 eV.

$\mathbf{k}$ is the electron crystal wave vector. We set $H_{\mathbf{k}0}$ as the nearest-neighbor tight binding Hamiltonian for the GG [3, 27, 28]

$$H_{\mathbf{k}0} = \begin{pmatrix} \Delta_g/2 & \gamma f(\mathbf{k}) \\ \gamma f^*(\mathbf{k}) & -\Delta_g/2 \end{pmatrix}, \tag{2}$$

where $\gamma = -3.03$ eV is the hopping integral,

$$f(\mathbf{k}) = \exp\left(\mathrm{i}\frac{ak_y}{\sqrt{3}}\right) + 2\exp\left(-\mathrm{i}\frac{ak_y}{2\sqrt{3}}\right)\cos\left(\frac{ak_x}{2}\right), \tag{3}$$

and $a = 2.46$ Å is the lattice constant.

The energies of CB and valence band (VB) are eigenvalues of $H_{\mathbf{k}0}$,

$$E_\alpha(\mathbf{k}) = \pm\sqrt{\gamma^2\left|f(\mathbf{k})\right|^2 + \Delta_g^2/4}\,, \tag{4}$$

where signs $\pm$ are for the CB ($\alpha = c$) and the VB ($\alpha = v$), respectively. The energy dispersion (4) is shown in Figure 1(c). Below we assume that initially (before the pulse) the VB is fully occupied and the CB is empty.

In solids, the applied electric field generates both the intraband (adiabatic) and interband (nonadiabatic) electron dynamics. The intraband dynamics is determined by the Bloch acceleration theorem [29], which describes the time evolution of the wave vector, $\mathbf{k}(t)$, in the time-dependent electric field, $\mathbf{F}(t)$,

$$\mathbf{k}(\mathbf{q}, t) = \mathbf{q} + \frac{e}{\hbar}\int_{-\infty}^{t}\mathbf{F}(t')\mathrm{d}t', \tag{5}$$

where $\mathbf{q}$ is the initial wave vector, $\mathbf{q} = \mathbf{k}(\mathbf{q}, -\infty)$.

The Bloch electron trajectories of Eq. (5) determine the separatrix, which is defined as a set of initial points $\mathbf{q}$ in the reciprocal space for which the electron trajectories pass precisely through the corresponding K or K' points [4]. It is a continuous line whose parametric equation is

$$\mathbf{q}(t) = \mathbf{K} - \mathbf{k}(0, t), \quad \text{or,} \quad \mathbf{q}(t) = \mathbf{K}' - \mathbf{k}(0, t), \tag{6}$$

where $t \in (-\infty, \infty)$ is a parameter. When the initial lattice momentum $\mathbf{q}$ is inside the separatrix, the corresponding Bloch trajectory, $\mathbf{k}(\mathbf{q}, t)$, encircles the K or K' point, otherwise it leaves the K or K' point outside.

The adiabatic solutions of Schrödinger Eq. (1), which means solutions within a single band α (without an interband coupling), are the well-known Houston functions [30],

$$\Phi^{(\mathrm{H})}_{\alpha\mathbf{q}}(\mathbf{r}, t) = \Psi^{(\alpha)}_{\mathbf{k}(\mathbf{q},t)}(\mathbf{r})\exp\left(\mathrm{i}\phi^{(\mathrm{D})}_\alpha(\mathbf{q}, t) + \mathrm{i}\phi^{(\mathrm{B})}_\alpha(\mathbf{q}, t)\right), \tag{7}$$

where $\alpha = v, c$ for the VB and CB, respectively, and $\Psi^{(\alpha)}_{\mathbf{k}}$ are the lattice-periodic Bloch functions in the absence of the pulse field. Here the dynamic phase, $\phi^{(\mathrm{D})}_\alpha$, and the geometric phase, $\phi^{(\mathrm{B})}_\alpha$, are defined as

$$\phi^{(\mathrm{D})}_\alpha(\mathbf{q}, t) = \frac{-1}{\hbar}\int_{-\infty}^{t}\mathrm{d}t'\left(E_\alpha[\mathbf{k}(\mathbf{q}, t')]\right), \tag{8}$$

$$\phi^{(\mathrm{B})}_\alpha(\mathbf{q}, t) = \frac{e}{\hbar}\int_{-\infty}^{t}\mathrm{d}t'\mathbf{F}\left(t'\right)\mathcal{A}^{\alpha\alpha}[\mathbf{k}(\mathbf{q}, t')], \tag{9}$$

where $\mathcal{A}^{\alpha\alpha} = \left\langle\Psi^{(\alpha)}_{\mathbf{q}}|\mathrm{i}\frac{\partial}{\partial\mathbf{q}}|\Psi^{(\alpha)}_{\mathbf{q}}\right\rangle$ is the intraband Berry connection.

The interband electron dynamics is determined by solutions of TDSE (1). Such solutions are parameterized by initial wave vector $\mathbf{q}$ and can be expanded in the basis of Houston functions $\Phi^{(\mathrm{H})}_{\alpha\mathbf{q}}(\mathbf{r}, t)$ as

$$\Psi_{\mathbf{q}}(\mathbf{r}, t) = \sum_{\alpha=c,v}\beta_{\alpha\mathbf{q}}(t)\Phi^{(\mathrm{H})}_{\alpha\mathbf{q}}(\mathbf{r}, t), \tag{10}$$

where $\beta_{\alpha\mathbf{q}}(t)$ are expansion coefficients.

It is convenient to introduce the following notations

$$\mathcal{D}^{\alpha\alpha_1}(\mathbf{q}, t) = \mathcal{A}^{\alpha\alpha_1}[\mathbf{k}(\mathbf{q}, t)] \times\exp\left(\mathrm{i}\phi^{(\mathrm{D})}_{\alpha\alpha_1}(\mathbf{q}, t) + \mathrm{i}\phi^{(\mathrm{B})}_{\alpha\alpha_1}(\mathbf{q}, t)\right), \tag{11}$$

$$\phi^{(\mathrm{D})}_{\alpha\alpha_1}(\mathbf{q}, t) = \phi^{(\mathrm{D})}_{\alpha_1}(\mathbf{q}, t) - \phi^{(\mathrm{D})}_{\alpha}(\mathbf{q}, t) \tag{12}$$

$$\phi^{(\mathrm{B})}_{\alpha\alpha_1}(\mathbf{q}, t) = \phi^{(\mathrm{B})}_{\alpha_1}(\mathbf{q}, t) - \phi^{(\mathrm{B})}_{\alpha}(\mathbf{q}, t) \tag{13}$$

$$\mathcal{A}^{\alpha\alpha_1}(\mathbf{q}) = \left\langle\Psi^{(\alpha)}_{\mathbf{q}}|\mathrm{i}\frac{\partial}{\partial\mathbf{q}}|\Psi^{(\alpha_1)}_{\mathbf{q}}\right\rangle, \tag{14}$$

where α and $\alpha_1 \neq \alpha$ are $\mathbf{v}$ or $\mathbf{c}$, $\mathcal{A}^{\alpha\alpha_1}(\mathbf{q})$ is the interband (non Abelian) Berry connection [2, 31, 32], $\phi^{(\mathrm{D})}_{\alpha\alpha_1}(\mathbf{q}, t)$ is the transition dynamic phase, and $\phi^{(\mathrm{B})}_{\alpha\alpha_1}(\mathbf{q}, t)$ is the transition Berry phase. Note that the interband dipole matrix element, $\mathbf{D}^{\alpha\alpha_1}(\mathbf{q})$, which determines the optical transitions between the VB and CB at a wave vector $\mathbf{q}$, is related to the transition Berry connection as $\mathbf{D}^{\alpha\alpha_1}(\mathbf{q}) = e\mathcal{A}^{\alpha\alpha_1}(\mathbf{q})$.

With these notations, the Schrödinger equation in the adiabatic basis of the Houston functions (interaction representation) takes the following form

$$\mathrm{i}\hbar\frac{\partial B_{\mathbf{q}}(t)}{\partial t} = H'(\mathbf{q}, t)B_{\mathbf{q}}(t), \tag{15}$$

where wave function (vector of state) $B_q(t)$ and Hamiltonian $H'(\mathbf{q}, t)$ are defined as

$$B_{\mathbf{q}}(t) = \begin{bmatrix}\beta_{c\mathbf{q}}(t) \\ \beta_{v\mathbf{q}}(t)\end{bmatrix}, \tag{16}$$

$$H'(\mathbf{q}, t) = -e\mathbf{F}(t)\hat{\mathcal{A}}(\mathbf{q}, t), \tag{17}$$

$$\hat{\mathcal{A}}(\mathbf{q},t)=\begin{bmatrix}0 & \mathcal{D}^{cv}(\mathbf{q},t)\\ \mathcal{D}^{vc}(\mathbf{q},t) & 0\end{bmatrix}. \tag{18}$$

Note that the interaction Hamiltonian, $H'(\mathbf{q},t)$, does not have the diagonal matrix elements, which is characteristic of the interaction representation.

We express a formal general solution of this equation in terms of the evolution operator, $\hat{S}(\mathbf{q},t)$, as follows

$$B_{\mathbf{q}}(t)=\hat{S}(\mathbf{q},t)B_{\mathbf{q}}(-\infty)\ ,$$
$$\hat{S}(\mathbf{q},t)=\hat{T}\ \exp\left[\mathrm{i}\int_{-\infty}^{t}\hat{\mathcal{A}}(\mathbf{q},t')\mathrm{d}\mathbf{k}(t')\right], \tag{19}$$

where $\hat{T}$ is the well-known time-ordering operator [33], and the integral is affected along the Bloch trajectory (Eq. (5)): $\mathrm{d}\mathbf{k}(t)=\frac{e}{\hbar}\mathbf{F}(t)\mathrm{d}t$. We solve Eq. (15) numerically for each value of the initial reciprocal wave vector, $\mathbf{q}$. From this solution we can find the electric current, $\mathbf{J}(t)=\{J_x(t),J_y(t)\}$, generated during the pulse.

2.2 Current

The 4-vector electric current density is defined as $\hat{j}=(e\hat{\rho},e\hat{\rho}\hat{\mathbf{v}})$, where $\hat{\rho}$ is the operator of charge density, and $\hat{\mathbf{v}}$ is the operator of velocity. The latter can be defined for a given lattice momentum $\mathbf{k}$ as

$$\hat{\mathbf{v}}_{\mathbf{k}}=\frac{i}{\hbar}\left[H_{\mathbf{k}0},\mathbf{r}\right]. \tag{20}$$

This can also be identically written as

$$\hat{\mathbf{v}}_{\mathbf{k}}=\frac{1}{\hbar}\left[\frac{\partial}{\partial\mathbf{k}},H_{\mathbf{k}0}\right]. \tag{21}$$

The band-nondiagonal ($\alpha\neq\alpha'$) matrix elements of the velocity can be found from Eq. (21) as

$$\left\langle\Psi^{(\alpha)}_{\mathbf{k}}\left|\hat{\mathbf{v}}_{\mathbf{k}}\right|\Psi^{(\alpha')}_{\mathbf{k}}\right\rangle=\frac{\mathrm{i}}{\hbar}\left[E_{\alpha}(\mathbf{k})-E'_{\alpha}(\mathbf{k})\right]\mathcal{A}^{\alpha\alpha'}(\mathbf{k}). \tag{22}$$

The band-diagonal matrix element of velocity can also be obtained from Eq. (21) taking into account an identity $\left[\frac{\partial}{\partial\mathbf{k}},H_{\mathbf{k}0}\right]=\left(\frac{\partial}{\partial\mathbf{k}}H_{\mathbf{k}0}\right)$ as

$$\left\langle\Psi^{(\alpha)}_{\mathbf{k}}\left|\hat{\mathbf{v}}_{\mathbf{k}}\right|\Psi^{(\alpha)}_{\mathbf{k}}\right\rangle=\mathbf{v}^{(g)}_{\alpha,\mathbf{k}}, \tag{23}$$

where $\mathbf{v}^{(g)}_{\alpha,\mathbf{k}}=\frac{\partial}{\partial\mathbf{k}}E_{\alpha}(\mathbf{k})$ is the group velocity in a band α at a lattice momentum $\mathbf{k}$.

The 2D current density in a crystal, $\mathbf{J}$ (called below current for brevity), is related to the electron velocity, $\mathbf{v}$ as $\mathbf{J}=\frac{e}{a^2}\mathbf{v}$, where a is the lattice constant (see Eq. (3)). This current, $\mathbf{J}$, is a sum of the interband and intraband contributions, $\mathbf{J}(t)=\mathbf{J}^{(\mathrm{intra})}(t)+\mathbf{J}^{(\mathrm{inter})}(t)$. In accord with Eq. (23), the intraband current can be expressed as

$$\mathbf{J}^{(\mathrm{intra})}(t)=\frac{2e}{a^2}\sum_{\alpha=\mathrm{c,v},\mathbf{q}}\left|\beta_{\alpha}(\mathbf{q},t)\right|^2\mathbf{v}^{(g)}_{\alpha,\mathbf{k}(\mathbf{q},t)}, \tag{24}$$

where a factor of 2 takes into the account spin degeneracy in our model where the spin–orbit interaction is not included. Similarly, in accord with Eq. (22), the interband current is given by

$$\begin{aligned}\mathbf{J}^{(\mathrm{inter})}(t)=\mathrm{i}\frac{2e}{\hbar a^2}\sum_{\substack{\mathbf{q}\\ \alpha,\alpha'=\mathrm{v,c}\\ \alpha\neq\alpha'}}&\beta^{*}_{\alpha'}(\mathbf{q},t)\beta_{\alpha}(\mathbf{q},t)\\ &\times\exp\{\mathrm{i}\phi^{(\mathrm{D})}_{\alpha'\alpha}(\mathbf{q},t)+\mathrm{i}\phi^{(\mathrm{B})}_{\alpha'\alpha}(\mathbf{q},t)\}\\ &\times\left[E_{\alpha'}\left(\mathbf{k}(\mathbf{q},t)\right)-E_{\alpha}\left(\mathbf{k}(\mathbf{q},t)\right)\right]\mathcal{A}^{\alpha\alpha'}\\ &\times\left(\mathbf{k}(\mathbf{q},t)\right).\end{aligned} \tag{25}$$

Note that the current is observable and, consequently, gauge-invariant despite the Berry connection being not gauge-invariant. This can be verified by using an explicit gauge transformation.

3 Results and discussion

3.1 Circularly polarized pulse

We apply an ultrafast chiral ("circularly-polarized") optical pulse, $\mathbf{F}=(F_x,F_y)$ whose waveform is symmetric with respect to a mirror reflection in the xz plane, $\mathcal{P}_{xz}$, as defined by the following parametrization

$$F_x=F_0(1-2u^2)\mathrm{e}^{-u^2}, \tag{26}$$

$$F_y=\pm 2F_0u\,\mathrm{e}^{-u^2}. \tag{27}$$

Here, F_0 is the amplitude of the pulse, $u=t/\tau$, where τ is a characteristic half-length of the pulse (in calculations, we choose $\tau=1$ fs), and $\pm$ determines the handedness: $+$ is for the right-handed and $-$ is for the left-handed chiral (circularly polarized) pulses. In this definition, the right-hand and left-hand pulses are $\mathcal{T}$-reversed with respect to each other. The waveforms of a right-hand pulse and a left-hand pulse are depicted in the insets in Figure 2(a) and (b), respectively.

We solve TDSE (1) numerically with initial conditions $\beta_{c\mathbf{q}}=0$ and $\beta_{v\mathbf{q}}=1$, i.e., the full VB and the empty CB. An optical pulse causes interband transitions and populates the CB. After the pulse, there is a stationary residual CB population remaining, $N^{(\mathrm{res})}_{\mathrm{CB}}(\mathbf{q})=|\beta_{c\mathbf{q}}(t=\infty)|^2$.

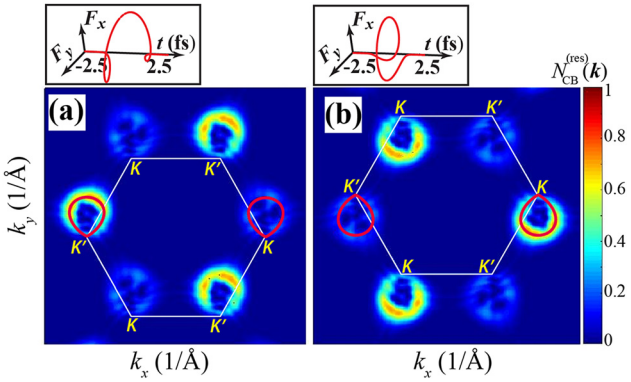

Figure 2: Residual CB population $N_{CB}^{(res)}(\mathbf{k})$ for GG with the band gap of 2 eV in the extended zone picture after a chiral single-cycle excitation pulse. (a) The excitation optical pulse is left-handed with the amplitude of $F_0 = 0.5$ V Å^{-1}. Inset: Waveform of the pulse $\mathbf{F}(t) = \{F_x(t), F_y(t)\}$ as a function of time t. (b) The excitation optical pulse is right-handed with the amplitude of $F_0 = 0.5$ V Å^{-1}. Inset: Waveform of the pulse as a function of time t. The solid white lines show the boundary of the first Brillouin zone with the K, K' points indicated. The separatrix (Eq. (6)) is shown in panels (a) and (b) by red solid lines.

For single-cycle left-handed and right-handed chiral pulses with the amplitude of 0.5 V Å^{-1} the distributions of the residual CB population for a GG with a bandgap of $\Delta_g = 2$ eV are shown in Figure 2(a) and (b), respectively. In a pristine graphene, $\Delta_g = 0$, a chiral pulse with a waveform symmetric with respect to the $\mathcal{P}_{xz}$ mirror reflection produces a strictly zero valley polarization [34], i.e., the K and K' valleys are populated equally. In sharp contrast, for a GG, there is a large valley polarization. This is because that for GG, the $\mathcal{P}_{xz}$ symmetry is broken. As a result, for a chiral pulse, which breaks down the time-reversal symmetry, the response of the GG in the K and K' valleys is different.

The different populations of the K and K' valley can be also understood from the properties of the interband coupling at two valleys. Namely, the fundamental evolution operator (19) can be rewritten in the form

$$\hat{S}(\mathbf{q}, t) = \hat{T} \exp\left[\mathrm{i}\int_{-\infty}^{t} \hat{\mathcal{A}}_{\parallel}(\mathbf{q}, t')\, \mathrm{d}k(t)\right], \tag{28}$$

where the longitudinal component of the non Abelian Berry connection is defined as $\hat{\mathcal{A}}_{\parallel}(\mathbf{q}, t) = \hat{\mathcal{A}}(\mathbf{q}, t)\mathbf{F}(t)/F(t)$, and $\mathrm{d}k(t) = \frac{e}{\hbar}F(t)\mathrm{d}t$. Explicitly, matrix $\hat{\mathcal{A}}_{\parallel}(\mathbf{q}, t)$ has the form

$$\hat{\mathcal{A}}_{\parallel}(\mathbf{q}, t) = \begin{bmatrix} 0 & \mathcal{D}_{\parallel}^{(\mathrm{cv})}(\mathbf{q}, t) \\ \mathcal{D}_{\parallel}^{(\mathrm{cv})*}(\mathbf{q}, t) & 0 \end{bmatrix}, \tag{29}$$

where

$$\mathcal{D}_{\parallel}^{(\mathrm{cv})}(\mathbf{q}, t) = \left|\mathcal{A}_{\parallel}^{(\mathrm{cv})}(\mathbf{k}(\mathbf{q}, t)\right| \exp\left[\mathrm{i}\phi_{\mathrm{cv}}^{(\mathrm{tot})}(\mathbf{q}, t)\right], \tag{30}$$

and the total phase, $\phi_{\mathrm{cv}}^{(\mathrm{tot})}$, is defined as

$$\begin{aligned} \phi_{\mathrm{cv}}^{(\mathrm{tot})}(\mathbf{q}, t) &= \phi_{\mathrm{cv}}^{(\mathrm{D})}(\mathbf{q}, t) + \phi_{\mathrm{cv}}^{(\mathrm{T})}; \\ \phi_{\mathrm{cv}}^{(\mathrm{T})} &= \phi_{\mathrm{cv}}^{(\mathrm{B})}(\mathbf{q}, t) + \phi_{\mathrm{cv}}^{(\mathrm{A})}(\mathbf{q}, t). \end{aligned} \tag{31}$$

Here, $\phi_{\mathrm{cv}}^{(\mathrm{T})}$ is the topological phase, and $\phi_{\mathrm{cv}}^{(\mathrm{A})}(\mathbf{q}, t) = \arg\left[\mathcal{A}_{\parallel}(\mathbf{q}, t)\right]$ is the phase of the interband coupling amplitude.

As we see from Eq. (30), the interband electron dynamics is determined by the total phase $\phi_{\mathrm{cv}}^{(\mathrm{tot})}$, which is a sum of the dynamic phase, $\phi_{\mathrm{cv}}^{(\mathrm{D})}$, and topological phase, $\phi_{\mathrm{cv}}^{(\mathrm{T})}$. The symmetry of the dynamic and topological phases with respect to the valley index (pseudospin) is opposite: The dynamic phase is even while the topological phase is odd. Assume that in one valley, say K, at an initial lattice momentum $\mathbf{q}$, the dynamic and topological phases have opposite signs and cancel one another. This is accord with Eq. (28) will lead to a coherent accumulation of transition amplitude and, consequently, a large population of the CB. At the same time, because of the valley antisymmetry of the topological phases, the dynamic and topological phases in valley K' will add to each other causing rapid oscillation of the integrand and mutual compensation of contributions over time in Eq. (28), leading to a low CB population. This is an effect of the topological resonance [34].

As one can see in Figure 2(a), for the left-handed chiral pulse, the topological resonance occurs in the K' valley. In contrast, for the right-handed chiral pulse, it takes place in the K valley (Figure 2(b)). Note that the conventional resonance can also be described as a cancellation of the dynamic phase $\phi_{\mathrm{cv}}^{(\mathrm{D})} \approx \Delta_g t/\hbar$ (where Δ_g is the bandgap) and the field phase $-\omega t$, which occurs for $\omega \approx \Delta_g/\hbar$. In sharp contrast to the topological resonance, the conventional resonance is symmetric with respect to the valley index.

The excitation pulses generate electric currents (see Eqs. (24) and (25)), which are experimentally observable – cf. Ref. [7]. In Figure 3, we show the x (longitudinal, i.e., along the maximum electric field of the pulse) and y (transverse) components of the current for the left-handed and right-handed chiral pulses with an amplitude of 0.5 V Å^{-1} calculated for different values of the bandgap, Δ_g. As one can see, both the longitudinal and transverse currents are generated. The magnitude of these currents decreases with the bandgap along with the corresponding reduction in the CB population. The longitudinal current, J_x, for graphene ($\Delta_g = 0$) does not have a ballistic (dc) component: After

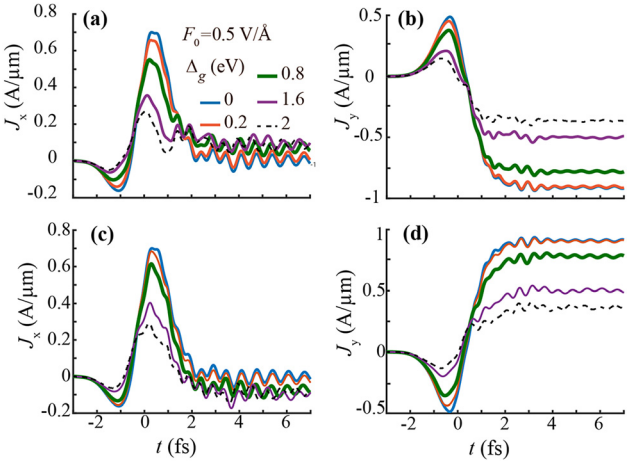

Figure 3: Currents J_x [panel (a)] and J_y [panel (b)] excited by a left-hand circularly polarized pulse with the amplitude of $F_0 = 0.5$ V Å^{-1}. The corresponding band gaps are marked in panel (a). In panels (c) and (d) the GG is excited by a right-hand circularly polarized pulse.

the pulse ends, only decaying oscillations due to interband contribution are present – see Figure 3(a) and (c). This is because the dc current is purely intraband (cf. Eqs. (24) and (25)) and, therefore, it is completely determined by the residual CB populations, which, for pristine graphene, are $\mathcal{P}_{yz}$-symmetric due to its inherent $\mathcal{P}_{xz}$ symmetry [34]. This results in a complete vanishing of the ballistic J_x current for pristine graphene. With the opening of the bandgap, the $\mathcal{P}_{xz}$ symmetry is broken, and there is a non-zero but still small ballistic current.

3.2 Linearly polarized probe and anomalous Hall effect

As described above in Section 3.1, a strong single-oscillation chiral pulse creates a large valley polarization in the GG , where the carriers predominantly occupy either K or K' valley as determined by the pulse's handedness. The resulting state has a broken $\mathcal{T}$ symmetry. A probe dc electric field applied to such a system will cause a Hall effect in the absence of any external or internal magnetic field, which is the anomalous Hall effect [35–38].

The anomalous Hall effect can be probed not only with a dc electric field but also with a linearly-polarized optical pulse applied after the strong ("pump") chiral pulse. However, in this case to have a finite transferred charge, the linearly-polarized pulse must be strong: cf.: For a weak pulse, the total transferred charge will be zero due to the temporal averaging. The anomalous Hall current generated by ultrafast linearly-polarized pulse is due to two factors: (i) Finite valley polarization of the GG and (ii) anisotropic CB population distribution around the K points. This is different from a dc electric field, for which the Hall current is generated because of the finite valley polarization only.

Correspondingly, we apply a nonlinear probe: A strong linearly-polarized pulse whose field is comparable to that of the chiral pulse, i.e., $\sim 0.1 - 0.5$ V Å^{-1}. For such a pulse, the optical nonlinearity (rectification) would define a predominant direction of the charge transfer both for longitudinal current (in the direction of the linear polarization) and for the transverse current (the anomalous Hall current). We consider a pulse linearly polarized along the y axis with the following waveform

$$F_x = 0, \quad F_y = F_1(1 - 2u^2)\mathrm{e}^{-u^2}, \tag{32}$$

where F_1 is the amplitude of the pulse. Note that for such a pulse in the absence of the valley polarization, there is only a longitudinal current J_y: A transverse current J_x is forbidden by the $\mathcal{P}_{yz}$ symmetry of the system.

We apply such a linearly-polarized pulse after the chiral pulse ends (i.e., at $t \geq 6$ fs). The resulting currents, which are calculated from Eqs. (24) and (25), are shown in Figure 4 where the strong probe pulse is applied with its center at $t = 8$ fs. Note that both the longitudinal current, J_y and the transverse (anomalous Hall) current J_x are present in the response.

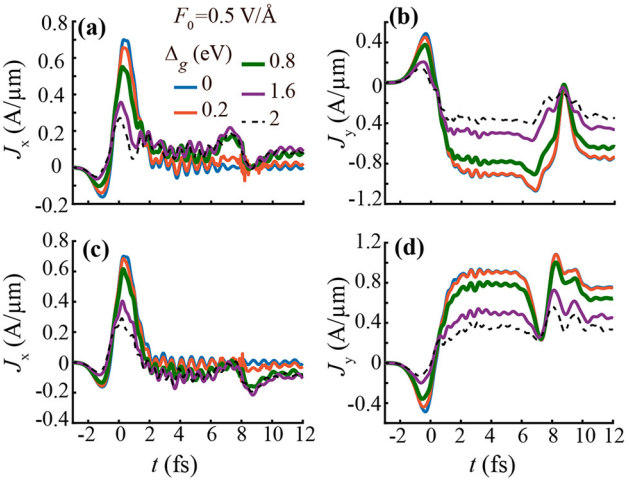

Figure 4: Electric currents J_x [panel (a)] and J_y [panel (b)] generated by a left-hand circularly polarized pulse (2 fs $\geq t \geq -2$ fs) followed by a linearly polarized pulse (10 fs $\geq t \geq 6$ fs). The amplitudes of circularly and linearly polarized pulses are the same, $F_0 = F_1 = 0.5$ V Å^{-1}. The corresponding band gaps are marked in panel (a). Panels (c) and (d) are the same as panels (a) and (b) but excited by a combination of right-hand circularly polarized pulse and a linear polarized pulse.

As we have already pointed out, the anomalous Hall current directly probes the valley polarization of the system. As one can see in Figure 4(a) and (c), for the pristine graphene ($\Delta_g = 0$), the Hall current, J_x, is precisely zero due to the absence of the valley polarization (the corresponding lines on the graphs do not change in response to the probe pulse whatsoever). With the bandgap increasing, the Hall current during the linearly polarized pulse, as expected, monotonically increases (Figure 4(a) and (c)) because the induced valley polarization increases with the bandgap. The anomalous Hall current, J_x, changes its sign with the chirality of the pump pulse as protected by the $\mathcal{T}$-reversal symmetry. This anomalous Hall current causes a net charge transfer in the x direction, which can be measured experimentally.

A remarkable property of the anomalous Hall current is that it has a very small ballistic component (that is the J_x current after the end of the probe pulse (Figure 4(a) and (c)), so it can be considered instantaneous (inertialess). To explain this, we consider symmetry of the optical waveforms applied to the system (both chiral and linearly polarized): It is $\mathcal{T}\mathcal{P}_{xz}$. For graphene, it is also the symmetry of the system. Thus for the graphene, the ballistic current is twice forbidden: The $\mathcal{T}\mathcal{P}_{xz}$ symmetry forbids the valley polarization by the applied chiral pulse, and it also directly forbids the J_x current because under it J_x transforms to $-J_x$. For the gapped (semiconductor) materials, the $\mathcal{P}_{xz}$ symmetry is not exact. Nevertheless, the ballistic anomalous Hall current, J_x, is still very small as our computations show. Concluding, the anomalous Hall current excited by a strong linearly-polarized probe pulse acting after the strong chiral pump pulse is ultrafast (existing predominantly within the duration of the probe pulse; it is odd (changes its sign) with respect to the pump chirality.

As one can see in Figure 4(b) and (c), the longitudinal current, J_y in response to the probe pulse monotonically decreases with the bandgap in accord with the decreasing CB population. Note that the J_y current exists even for pristine graphene. Both components J_x and J_y generated in response to the strong probe pulse increase with its amplitude – see Figure 5.

We estimate an effective Hall conductivity as $\sigma_{xy} = \Delta J_x/\Delta F_1$, where $\Delta J_x \sim 0.3\ \frac{A}{\mu m}$, and $\Delta F_1 \sim 2$ V Å^{-1}, where both ΔF_1 and ΔJ_x are obtained from Figure 5 as the full range of the change of the corresponding quantity for field $F_1 = 1\ \frac{V}{A}$. Using these values, we estimate the effective Hall conductivity as $\sigma_{xy} \sim 0.2G_0$, where $G_0 = \frac{e^2}{\pi\hbar}$ is the conductance quantum.

The classical Hall conductivity is $\sigma_{xy} = enc/B$, where n is the 2D electron density, c is speed of light, and B is the magnetic field. We may express it in terms of an effective magnetic field, B_{eff}, which yields the same magnitude of σ_{xy} as the anomalous Hall conductance, $\sim 0.2G_0$. An estimate is $B_{\text{eff}} = enc/\sigma_{xy} \sim 10^9$ G $= 10^5$ T, which is a gigantic magnetic field. Consequently, the predicted anomalous all-optical Hall effect is extraordinarily strong. It can serve as an efficient source of ultrafast currents providing a direct access to the ultrafast topological charges induced in the system.

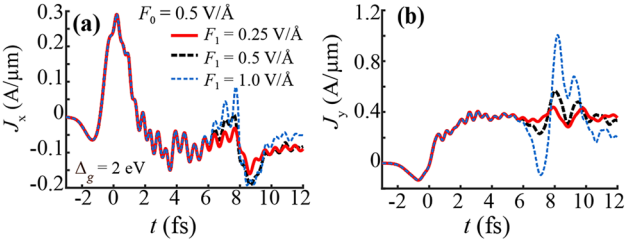

Figure 5: Electric currents J_x [panel (a)] and J_y [panel (b)] generated by a left-hand circularly polarized pulse (2 fs $\geq t \geq -2$ fs) followed by a linearly polarized pulse (10 fs $\geq t \geq$ 6 fs). The amplitude of the circularly polarized pulse is $F_0 = 0.5$ V Å^{-1}, while the corresponding amplitudes of the linearly polarized pulse are marked in panel (a). The band gap is 2 eV.

4 Conclusion

A gigantic ultrafast all-optical anomalous Hall effect occurs when two strong single-oscillation optical pulses are applied to the GG or similar hexagonal-symmetry semiconductor materials such as TMDCs or h-BN. These materials possess a broken inversion symmetry and a finite direct bandgap. The two pulses, which generate the anomalous ultrafast Hall effect, are a sequence of a single-cycle chiral pulse followed by a single-cycle linearly-polarized pulse. The chiral pulse breaks down the $\mathcal{T}$-reversal symmetry inducing a strong valley polarization, which effectively plays the role of an effective magnetic field. The induction of the strong valley polarization by a fundamentally fastest single oscillation chiral pulse is due to the recently predicted phenomenon of topological resonance. This is a wide-bandwidth, ultrafast effect, which is due to the mutual cancellation of the topological and dynamic phases. The topological resonance is independent of spin of electron and depends on a purely orbital dynamics of electrons in the gapped hexagonal-symmetry monolayers. The valley polarization induced by a conventional method through selective population of the valleys by a continuous circularly polarized pulse is due to different symmetries

of the interband dipole matrix elements at the K and K' points. Namely the dipole matrix elements are of the D_+ and D_- types, i.e., they have different phases, at the K and K' points. Thus the fundamental difference between the conventional valley selective population and the population due to topological resonance is that the topological resonance is due to *dynamical variation* of the phase of the interband dipole matrix elements and the geometric phase of the wavefunctions, i.e., total topological phase, which competes with the dynamics phase. Since the net interband electron dynamics in the field of an ultrashort pulse is due to both phase accumulation and the dipole matrix elements, both the conventional valley selection rule and the selection rule due to topological resonance contribute to the valley polarization.

The subsequent application of a strong single-oscillation probe pulse that is linearly-polarized along the armchair edge (y axis) to such a system, which acquired chirality (a large valley polarization), produces a Hall current in the zigzag direction (x axis) transverse to the polarization of the probe pulse.

In our approach we used a single oscillation linearly polarized pulse to probe the valley polarization of the system. The valley degree of freedom can be also probed by a long laser pulse [39]. In this case the response of the electron system and the corresponding anomalous Hall current depend on the relation between the carrier relaxation time and the period of the pulse.

The fundamental distinction and advantage of this proposed all-optical anomalous Hall effect in 2D hexagonal semiconductors from the recent proposal [40] and observation [38] of a light-induced anomalous Hall effect in graphene is that ours is the fundamentally fastest anomalous effect possible in nature: It takes just a single optical period to induce the strong valley polarization and just one other optical period to read it out. Such a read out can fundamentally be done either by recording the charge transferred after the probe pulse or by observing a THz radiation emitted by the Hall current that is polarized in the x direction. In sharp contrast, in Ref. [38] the chiral excitation pulse was orders of magnitude less intense and longer: Its duration was ≈ 500 fs, i.e., in the picosecond range vs. our pulse of just $\lesssim 5$ fs duration; the read out was electrical.

There is another fundamental distinction of our predicted effect from Refs. [38, 40]. Namely, a possibility to induce the strong valley polarization by a pulse with just a single optical cycle is due to the effect of topological resonance that exists only in gapped materials such as GG and 2D semiconductors (TMDCs and h-BN) but not in graphene. Therefore use of a much longer picosecond (quasi-CW) pulses in Refs. [38, 40] is necessary; graphene cannot possess a single-cycle anomalous all-optical Hall effect.

The predicted ultrafast anomalous all-optical Hall effect has a potential to have applications in ultrafast memory and information processing, both classical and quantum.

Acknowledgments: We acknowledge fruitful discussions with Prof. M. I. Stockman.

Author contribution: All the authors have accepted responsibility for the entire content of this submitted manuscript and approved submission.

Research funding: Major funding was provided by Grant No. DE-SC0007043 from the Materials Sciences and Engineering Division of the Office of the Basic Energy Sciences, Office of Science, US Department of Energy. Numerical simulations were performed using support by Grant No. DE-FG02-01ER15213 from the Chemical Sciences, Biosciences and Geosciences Division, Office of Basic Energy Sciences, Office of Science, US Department of Energy. The work of V.A. was supported by NSF EFRI NewLAW Grant No. EFMA-1741691.

Conflict of interest statement: The authors declare no conflicts of interest regarding this article.

References

[1] K. S. Novoselov, A. Mishchenko, A. Carvalho, and A. H. C. Neto, "2D materials and van der Waals heterostructures," *Science*, vol. 353, pp. 461–1, 2016.

[2] D. Xiao, M.-C. Chang, and Q. Niu, "Berry phase effects on electronic properties," *Rev. Mod. Phys.*, vol. 82, pp. 1959–2007, 2010.

[3] T. G. Pedersen, A.-P. Jauho, and K. Pedersen, "Optical response and excitons in gapped graphene," *Phys. Rev. B*, vol. 79, p. 113406, 2009.

[4] H. K. Kelardeh, V. Apalkov, and M. I. Stockman, "Attosecond strong-field interferometry in graphene: chirality, singularity, and Berry phase," *Phys. Rev. B*, vol. 93, p. 155434, 2016.

[5] S. A. O. Motlagh, J.-S. Wu, V. Apalkov, and M. I. Stockman, "Femtosecond valley polarization and topological resonances in transition metal dichalcogenides," *Phys. Rev. B*, vol. 98, 2018, Art no. 081406(R).

[6] H. K. Kelardeh, V. Apalkov, and M. I. Stockman, "Graphene in ultrafast and superstrong laser fields," *Phys. Rev. B*, vol. 91, 2015, Art no. 045439.

[7] T. Higuchi, C. Heide, K. Ullmann, H. B. Weber, and P. Hommelhoff, "Light-field-driven currents in graphene," *Nature*, vol. 550, pp. 224–228, 2017.

[8] D. Xiao, G. B. Liu, W. X. Feng, X. D. Xu, and W. Yao, "Coupled spin and valley physics in monolayers of MoS_2 and other

group-VI dichalcogenides,'' *Phys. Rev. Lett.*, vol. 108, 2012. https://doi.org/10.1103/PhysRevLett.108.196802.
[9] H. L. Zeng, J. F. Dai, W. Yao, D. Xiao, and X. D. Cui, ''Valley polarization in MoS_2 monolayers by optical pumping,'' *Nat. Nanotechnol.*, vol. 7, pp. 490–493, 2012.
[10] K. F. Mak, K. L. He, J. Shan, and T. F. Heinz, ''Control of valley polarization in monolayer MoS_2 by optical helicity,'' *Nat. Nanotechnol.*, vol. 7, pp. 494–498, 2012.
[11] T. Cao, G. Wang, W. P. Han, et al., ''Valley-selective circular dichroism of monolayer molybdenum disulphide,'' *Nat. Commun.*, vol. 3, pp. 1–5, 2012.
[12] A. M. Jones, H. Y. Yu, N. J. Ghimire, et al., ''Optical generation of excitonic valley coherence in monolayer WSe_2,'' *Nat. Nanotechnol.*, vol. 8, pp. 634–638, 2013.
[13] E. J. Sie, J. McIver, Y. H. Lee, L. Fu, J. Kong, and N. Gedik, ''Valley-selective optical Stark effect in monolayer WS_2,'' *Nat. Mater.*, vol. 14, pp. 290–294, 2015.
[14] E. H. Hall, ''On a new action of the magnet on electric currents,'' *Am. J. Math.*, vol. 2, pp. 287–292, 1879.
[15] N. Nagaosa, J. Sinova, S. Onoda, A. H. MacDonald, and N. P. Ong, ''Anomalous hall effect,'' *Rev. Mod. Phys.*, vol. 82, pp. 1539–1592, 2010.
[16] K. F. Mak, K. L. McGill, J. Park, and P. L. McEuen, ''The valley hall effect in MoS_2 transistors,'' *Science*, vol. 344, pp. 1489–1492, 2014.
[17] P. X. Nguyen and W.-K. Tse, ''Photoinduced anomalous hall effect in two-dimensional transition metal dichalcogenides,'' *Phys. Rev. B*, vol. 103, p. 125420, 2021.
[18] Xi. Dai and F.-C. Zhang, ''Light-induced hall effect in semiconductors with spin-orbit coupling,'' *Phys. Rev. B*, vol. 76, 2007, Art no. 085343.
[19] D. Jariwala, A. Srivastava, and P. M. Ajayan, ''Graphene synthesis and band gap opening,'' *J. Nanosci. Nanotechnol.*, vol. 11, pp. 6621–6641, 2011.
[20] M. S. Nevius, M. Conrad, F. Wang, et al., ''Semiconducting graphene from highly ordered substrate interactions,'' *Phys. Rev. Lett.*, vol. 115, p. 136802, 2015.
[21] E. H. Hwang and S. Das Sarma, ''Single-particle relaxation time versus transport scattering time in a two-dimensional graphene layer,'' *Phys. Rev. B*, vol. 77, p. 195412, 2008.
[22] M. Breusing, S. Kuehn, T. Winzer, et al., ''Ultrafast nonequilibrium carrier dynamics in a single graphene layer,'' *Phys. Rev. B*, vol. 83, p. 153410, 2011.
[23] E. Malic, T. Winzer, E. Bobkin, and A. Knorr, ''Microscopic theory of absorption and ultrafast many-particle kinetics in graphene,'' *Phys. Rev. B*, vol. 84, p. 205406, 2011.
[24] D. Brida, A. Tomadin, C. Manzoni, et al., ''Ultrafast collinear scattering and carrier multiplication in graphene,'' *Nat. Commun.*, vol. 4, p. 1987, 2013.
[25] I. Gierz, J. C. Petersen, M. Mitrano, et al., ''Snapshots of non-equilibrium Dirac carrier distributions in graphene,'' *Nat. Mater.*, vol. 12, pp. 1119–24, 2013.
[26] A. Tomadin, D. Brida, G. Cerullo, A. C. Ferrari, and M. Polini, ''Nonequilibrium dynamics of photoexcited electrons in graphene: collinear scattering, Auger processes, and the impact of screening,'' *Phys. Rev. B*, vol. 88, 2013, Art no. 035430.
[27] S. Y. Zhou, G. H. Gweon, A. V. Fedorov, et al., ''Substrate-induced bandgap opening in epitaxial graphene,'' *Nat. Mater.*, vol. 6, p. 770, 2007.
[28] P. K. Pyatkovskiy, ''Dynamical polarization, screening, and plasmons in gapped graphene,'' *J. Condens. Matter Phys.*, vol. 21, 2008, Art no. 025506.
[29] F. Bloch, ''Über die Quantenmechanik der Elektronen in Kristallgittern,'' *Z. Phys.*, vol. 52, pp. 555–600, 1929.
[30] W. V. Houston, ''Acceleration of electrons in a crystal lattice,'' *Phys. Rev.*, vol. 57, pp. 184–186, 1940.
[31] F. Wilczek and A. Zee, ''Appearance of gauge structure in simple dynamical systems,'' *Phys. Rev. Lett.*, vol. 52, pp. 2111–2114, 1984.
[32] F. Yang and R. B. Liu, ''Nonlinear optical response induced by non-Abelian Berry curvature in time-reversal-invariant insulators,'' *Phys. Rev. B*, vol. 90, p. 245205, 2014.
[33] A. A. Abrikosov, L. P. Gorkov, and I. E. Dzialoshinskii, *Methods of Quantum Field Theory in Statistical Physics*, New York, Dover Publications, 1975.
[34] S. A. O. Motlagh, F. Nematollahi, V. Apalkov, and M. I. Stockman, ''Topological resonance and single-optical-cycle valley polarization in gapped graphene,'' *Phys. Rev. B*, vol. 100, p. 115431, 2019.
[35] N. Nagaosa, J. Sinova, S. Onoda, A. H. MacDonald, and N. P. Ong, ''Anomalous Hall effect,'' *Rev. Mod. Phys.*, vol. 82, pp. 1539–1592, 2010.
[36] M. Onoda and N. Nagaosa, ''Quantized anomalous Hall effect in two-dimensional ferromagnets: quantum Hall effect in metals,'' *Phys. Rev. Lett.*, vol. 90, p. 206601, 2003.
[37] C. Z. Chang, J. S. Zhang, X. Feng, et al., ''Experimental observation of the quantum anomalous Hall effect in a magnetic topological insulator,'' *Science*, vol. 340, pp. 167–170, 2013.
[38] J. W. McIver, B. Schulte, F. U. Stein, et al., ''Light-induced anomalous hall effect in graphene,'' *Nat. Phys.*, vol. 16, pp. 38–41, 2020.
[39] Y. Kim and J. D. Lee, ''Anomalous electron dynamics induced through the valley magnetic domain: a pathway to valleytronic current processing,'' *Nano Lett.*, vol. 19, pp. 4166–4173, 2019.
[40] S. A. Sato, P. Tang, M. A. Sentef, U. D. Giovannini, H. Hübener, and A. Rubio, ''Light-induced anomalous hall effect in massless Dirac fermion systems and topological insulators with dissipation,'' *New J. Phys.*, vol. 21, 2019, Art no. 093005.